Published in final edited form as:
IEEE J Sel Top Quantum Electron. 2010 March 1; 16(3): 530–544.

Optical assessment of tumor resection margins in the breast

J. Quincy Brown,
Dept. of Biomedical Engineering, Duke University, Durham, NC 27708 USA

Torre M. Bydlon,
Dept. of Biomedical Engineering, Duke University, Durham, NC 27708

Lisa M. Richards,
Dept. of Biomedical Engineering, Duke University, Durham, NC 27708

Bing Yu,
Dept. of Biomedical Engineering, Duke University, Durham, NC 27708

Stephanie A. Kennedy,
Dept. of Biomedical Engineering, Duke University, Durham, NC 27708

Joseph Geradts,
Depts. of Surgery, Pathology, and Biostatistics, respectively; Duke University Medical Center, Durham, NC 27708 USA

Lee G. Wilke,
Depts. of Surgery, Pathology, and Biostatistics, respectively; Duke University Medical Center, Durham, NC 27708 USA

Marlee Junker,
Dept. of Biomedical Engineering, Duke University, Durham, NC 27708

Jennifer Gallagher,
Depts. of Surgery, Pathology, and Biostatistics, respectively; Duke University Medical Center, Durham, NC 27708 USA

William Barry, and
Depts. of Surgery, Pathology, and Biostatistics, respectively; Duke University Medical Center, Durham, NC 27708 USA

Nimmi Ramanujam[Member, IEEE]
Dept. of Biomedical Engineering, Duke University, Durham, NC 27708

J. Quincy Brown: quincy.brown@duke.edu

Abstract

Breast conserving surgery, in which the breast tumor and surrounding normal tissue are removed, is the primary mode of treatment for invasive and *in situ* carcinomas of the breast, conditions that affect nearly 200,000 women annually. Of these nearly 200,000 patients who undergo this surgical procedure, between 20–70% of them may undergo additional surgeries to remove tumor that was left behind in the first surgery, due to the lack of intra-operative tools which can detect whether the boundaries of the excised specimens are free from residual cancer. Optical techniques have many attractive attributes which may make them useful tools for intra-operative assessment of breast tumor resection margins. In this manuscript, we discuss clinical design criteria for intra-operative breast tumor margin assessment, and review optical techniques appied to this problem. In addition, we report on the development and clinical testing of quantitative diffuse reflectance imaging (Q-DRI) as a potential solution to this clinical need. Q-DRI is a spectral imaging tool which has been applied to 56 resection margins in 48 patients at Duke University Medical Center. Clear sources of

contrast between cancerous and cancer-free resection margins were identified with the device, and resulted in an overall accuracy of 75% in detecting positive margins.

I. Introduction

A screening mammogram, which is recommended as an annual test for women over 40 years, is often the first step in detecting breast cancer. A woman with a suspicious mammogram typically undergoes an image guided needle biopsy procedure and histopathologic diagnosis of the core tissue to determine if she has cancer. Women diagnosed with stage 0, I, or II breast cancer who choose to retain their breast undergo breast conserving surgery (BCS) also known as a partial mastectomy or lumpectomy. Of the approximately 250,000 women diagnosed with breast cancer, most are eligible for BCS and approximately 165,000–180,000 women undergo this surgical procedure annually [1]. A good cosmetic outcome is a readily achievable goal with BCS.

In BCS, the surgeon attempts to resect the tumor with a surrounding rim of normal tissue while preserving as much of the normal tissue as possible. After surgery is completed, the specimen is submitted to pathology and the excised tissue is evaluated to determine if the margin is clear or positive. If the margin is positive or “close” (meaning cancer is present within a few mm of the surface), then the patient is advised to undergo re-excision surgery to achieve a clear margin. The criterion for a clear margin varies between institutions, but most centers deem a clear margin of 2 mm sufficient to avoid re-excision. A critical aspect of BCS is to orient the specimen accurately, such that the surgeon knows where to re-excise if the post-operative pathology report indicates that a margin is positive or close for tumor cells. For the purposes of specimen orientation, the lumpectomy specimen is viewed as a cube. The surgeon orients the specimen by putting sutures and/or surgical clips at the center of 4 of the 6 margins (anterior, posterior, inferior, superior, medial, and lateral). This orientation is maintained in the pathology lab by differential inking of the four surfaces. At Duke University Medical Center, breast margins are considered negative for residual carcinoma if there is at least 2 mm of normal tissue bordering the specimen. Thus, the margin may be classified as positive (tumor extending to the inked surface) (Fig. 1(A)), close (tumor within 2 mm of the margin) (Fig. 1(B)), or negative (tumor more than 2 mm from the margin) (Fig. 1(C)), and furthermore whether margin involvement is focal or extensive. From a patient management perspective, both a positive and a close margin require re-excision. Thus, if one of the margins is found to be positive or close by the pathologist, the surgeon knows which aspect of the lumpectomy cavity needs to be re-excised. The above approach is sufficiently effective to ensure complete excision of the positive margin in the second surgery in the majority of cases [2].

Apart from unnecessary re-excision surgeries, there are other compelling reasons to avoid positive margins at the primary BCS procedure. The pathologic margin status is an important predictor of local recurrence (LR) of an invasive or in-situ cancer after BCS. In a study of 341 women with BCS, 1.8% experienced a local recurrence if their specimen margins were negative. Patients with close (< 2mm) margins had a LR rate of 8.4% [3]. Thus, BCS’s achieving ≥ 2 mm tumor-free margins resulted in decreased local regional recurrence rates [3]. In a retrospective study of 1360 women who underwent BCS in the Netherlands from 1980 and 1994, inclusive of standard post-surgical radiation therapy, LR was found to be a major predictor for metastases and death [4].

Currently, surgeons do not have adequate intra-operative assessment tools to ensure that the cancer has been completely removed at the time of first surgery. The lack of this capability represents a significant unmet clinical need. Women who undergo repeat surgeries are

typically subject to pain, suffering, and disfigurement. The lack of an adequate intra-operative assessment tool results in 20–70% [5–14] of women needing to return for re-excision surgery because their tumor was not completely removed at their primary surgery. Only a small number of hospitals who perform BCS currently utilize intra-operative cytologic or pathologic analysis of tumor margins. Touch-prep or imprint cytology allows for cytologic evaluation of the whole lumpectomy surface and has good sensitivity and specificity [15]. It has been suggested by the Moffitt group that it can reduce operative time and re-excision rate [16]. However, this technique is time consuming, requires special expertise, and does not detect tumor foci close to the lumpectomy surface (residual cells < 2mm from the margin). Frozen section analysis is a technically challenging procedure due to the significant amount of fatty tissue found in breast specimens. While the best results using this technique have been shown to reduce the rate of second operations to about 20% [9], false negatives occur at high frequencies [17–19]. The vast majority of hospitals in the U.S. do not rely on intra-operative margin assessment by a pathologist.

According to interviews with leading surgeons and consultation with in-house medical experts, surgeons need a device that (1) will cut their repeat surgery rate by more than 50%, (2) takes less than 20 min to display a result, (3) has a sensing depth of 1–2 mm, (4) ideally surveys the entire surface of the tumor, (5) is usable on fatty tissues, and (6) does not require specialized personnel such as pathologists. Thus, there is a clear clinical need for a technology for breast tumor margin assessment, which can rapidly and objectively evaluate tumor margins, with a performance that meets these clinical criteria. Optical technologies have many attributes that make them attractive for such applications, in particular, the sensitivity of the techniques to physiological, chemical, and morphological changes associated with cancer, as well as sensing depths which are comparable to the criteria for clear margins.

II. Clinical Criteria for Breast Margin Assessment

In choosing or designing optical systems for tumor margin assessment, it is important to consider the sensing depth requirements for the particular organ site of interest. For example, the depth criterion for a ‘close’ margin in the brain requiring re-excision is typically more aggressive (shallower), since unnecessary removal of normal brain tissue may result in significant neurological defects. However, the criterion for a ‘close’ margin in the breast requiring re-excision is more conservative (deeper), since there are fewer disadvantages to removing additional normal tissue in that organ. Even within an organ site, the disease type may dictate the minimum acceptable distance of disease from the margin; for example, it may be preferable to have a deeper disease-free margin in breast cancer patients with ductal carcinoma *in situ* (DCIS) as opposed to those with invasive ductal carcinoma (IDC), due to the diffuse nature of DCIS which makes pathologic confirmation of a clean margin particularly difficult.

Although the definition of a clear margin varies by organ site and institution, the most common accepted pathologic criterion for a negative margin in the breast is a full 2 mm thick rim of normal tissue surrounding the excised tumor. The sensing depth of light varies from several millimeters in the UV-visible spectrum to several centimeters in the NIR region [20]. In the UV-visible region, tissues are absorption dominant, which restricts the penetration depth. With increasing wavelength, the overall absorption coefficient decreases and the ratio of scattering to absorption coefficients increase. Within each particular wavelength range, the sensing depth may be varied (within fundamental limits) by careful selection of illumination-collection geometry. For instance, in fiber-based optical spectroscopy, selection of short separation distances between illumination and collection fibers will select for sensing depths on the shallower end of the range, whereas longer

source-detector separations will select for sensing depths at the deeper end of the range. These generalizations hold for steady-state spectroscopies, but may differ depending on the technology. For example, the use of coherence-gating in OCT means that multiply-scattered photons are rejected, and sensing depths of 2–3 mm are achieved only with the use of longer, NIR wavelengths where the scattering probability is lowest.

The decision of whether to survey the excised specimen, or the tumor cavity *in vivo*, also has significant bearing on the system design, since the required performance characteristics would be drastically different in either case. Analysis of the tissue *in vivo* would suggest an extremely shallow sensing depth, since the goal is to be sensitive to only the most superficial layer of tissue where residual cancer is found, whereas analysis of the tissue *ex vivo* would require a sensing depth that is equivalent to the clinical definition of a 'close' margin, since this approach confers the advantage of being able to detect these close margins which also require re-excision.

Another important clinical criterion for tumor margin assessment is sufficient area sampling within practical time constraints. The size of resected tumor specimens (or resection cavities) varies depending on the organ site, but can be quite large, for instance in the breast. Fig. 2 contains a histogram of single margin surface areas from 120 patients enrolled for optical breast studies at our institution. As seen in the figure, the most common single margin area is about 20 cm^2, whereas the range of sizes is from 5 cm^2 to over 40 cm^2. Considering that these numbers are for single margins only (one of a total of 6 margins), it is not unreasonable to expect an excised BCS specimen to have a total surface area of upwards of 100 cm^2. As such, a critical design criterion for optical margin assessment devices must be the ability to be adapted to a wide range of margin sizes, as well as to be able to quickly sample even the largest margins. In order for intra-operative assessment of tumor margins to be useful clinically, the methodology must be capable of surveying the majority of the tissue surface within 20–40 minutes, which is the time range occupied by current intra-operative pathology methods. Due to the high cost of OR time, methods which take longer than 40 minutes to cover the majority of the specimen or cavity surface will not be acceptable clinically. These collective issues must all be considered carefully in the selection and design of the optimized system, to ensure that the device performance is compatible with currently accepted clinical paradigms and to maximize clinical benefit of the device.

III. Optical Methods for Breast Margin Assessment

Table 1 contains a summary and comparison of clinical studies reported in the literature, in which various optical techniques were applied to the detection or demarcation of tumor margins in the breast. The aspects of each study, relevant to the clinical considerations given above, are listed in the table. Each of these studies will be discussed in the context of the optical technique used.

One of the earliest studies on the use of optical spectroscopy for characterization of breast resection tumor margins was by Bigio et al. [21]. In this work, the authors used elastic-scattering spectroscopy (ESS, a variant of diffuse reflectance spectroscopy) in the UV-Visible range. The diffuse reflectance spectrum is a function of the optical absorption and scattering coefficient spectra [22]. The shape and magnitude of the absorption coefficient depends on the extinction coefficient and concentrations, respectively of dominant tissue chromophores which include oxygenated hemoglobin (HbO_2) and deoxygenated hemoglobin (Hb), and β-carotene in the UV-VIS spectrum [23,24]. The optical scattering coefficient is known to be sensitive to the spatial architecture and organization of the tissue [25–27]. In the study by Bigio et al., a single fiber-optic probe assembly, with a sensing depth of 300 μm, was used to measure diffuse reflectance spectra from the tumor cavity *in*

vivo after resection, followed by biopsy of the measured tissue for pathologic correlation. The goal of intra-cavity measurements was to detect any residual foci of cancer *at the surface* of the resection margin hence the shallow sensing depth of 300 μm was appropriate for this purpose. Normalized spectra were divided into 20 nm intervals, and interval integral intensities were used as input parameters to classification algorithms (including artificial neural networks and hierarchical cluster analysis). With the use of an artificial neural network, the investigators demonstrated a best (non cross-validated) classification sensitivity and specificity of 69% and 85%, respectively. This work was important in that it represented initial evidence that optical spectroscopy was sensitive to absorption and/or scattering changes which accompany the presence of cancer.

Similarly to the Bigio et al. study, Haka and co-workers [28] used Raman spectroscopy to examine the tumor resection cavity *in vivo*. Raman spectroscopy (RS) is a form of vibrational spectroscopy, in which monochromatic excitation light is inelastically scattered from molecules excited by the incident light. In the so-called “fingerprint region,” which extends from 500–2000 cm^{-1}, Raman spectroscopy can be used to identify the contributions of a number of organic molecules which have been shown to be representative of sources of contrast in breast cancer (for instance, fat, collagen, cell cytoplasm and nucleus) [29]. NIR light is typically used in the excitation of Raman signals in tissue, which increases the sensing depth of the technique (up to 1 mm) but results in signals that are very weak in nature. In the study by Haka et al., a 2 mm diameter fiber optic probe was used to collect Raman spectra from 30 tissue sites (29 benign and normal, 1 cancer) from 9 patients. Feature extraction was accomplished by fitting the Raman spectra, to a linear combination of spectra from various breast tissue constituents, and retaining the resulting fit coefficients. Use of these predictors (fit coefficients) in a logistic regression classification algorithm trained on a previous (*ex vivo*) dataset [30] resulted in a sensitivity and specificity of 100% and 100%, respectively. These studies served to show the association between spectroscopic measurements and tissue pathology. However, these studies were not designed to do a true assessment of the surgical margin, which requires imaging of the area of interest, such that the overall surgical margin status as determined by histopathology (negative, close, or positive) could be used as the end-point for comparison to the optical results.

In another application of Raman spectroscopy to breast tumor margin assessment, Marzullo et al. [31] used FT-Raman spectroscopy (FT-RS) to evaluate the borders of IDC in excised breast tissues. Special care was taken to select a small piece of the margin that may contain residual carcinoma, and the device was scanned over a 1 mm^3 tissue volume in 6 minutes, on previously frozen and thawed tissues. Measured spectra were compared to the histological analysis of the measured tissue sites. The authors found that the borders of infiltrating lesions had FT-Raman spectra similar to those of normal tissues, with the exception of a peak at 538 cm^{-1} which corresponded to the disulfide bridges in cysteine. In an interesting study by Keller et al. [32], a variant of Raman spectroscopy, spatially-offset Raman spectroscopy (SORS), was used to investigate the utility of the method in detecting cancer beneath a layer of normal tissue (the model of a “close” margin). The authors created a model breast tumor margin by sandwiching various thicknesses of normal tissue above cancer tissue, using glass coverslips between the layers. A systematic investigation of the effect of varying source-detector separation as well as the thickness of the upper layer of normal tissue provided an analysis of the ability of the method to detect cancer beneath the tissue surface. At a source detector separation of 4 mm, the device was able to detect residual cancer up to 2 mm below the tissue surface, which would meet the requirements of detection of a close margin clinically in the breast.

The collective studies described above demonstrate that both diffuse reflectance and Raman spectroscopy show optical sources of contrast that are potentially useful for intra-operative

margin assessment. These methods could be useful if properly scanned or multiplexed to provide increased tissue coverage to survey the full margin.

An interesting application within the last three years has been the use of optical coherence tomography (OCT) for breast margin assessment. OCT can perform high resolution, cross-sectional tomographic imaging of the internal microstructure, particularly refractive index discontinuities, of turbid media, such as biological tissue [33]. OCT uses low-coherence interferometry (or white-light interferometry) with a low-coherence, broadband light source (or wavelength tunable laser) to measure backscattered or back reflected light, thus an image resolution of sub-micrometer can be achieved with a very large source spectral width. Most OCT systems operate in the near-infrared band with a penetration depth up to a few millimeters. In time domain OCT, an A-scan (z-axis) is obtained by varying the optical path-length of the reference arm, whereas in frequency-domain OCT, the A-scan can be immediately calculated by a Fourier-transform from the acquired spectra, without movement of the reference arm [34]. Two- and three- dimensional images are typically obtained by mechanical scanning laterally, but recently developed parallel OCT schemes eliminate the need for lateral scanning and, therefore, dramatically increase the imaging rate [35]. Initially developed for retinal imaging, OCT systems are now commercially available and have found application in a number of medical and surgical specialties, including ophthalmology, gastroenterology, dermatology, cardiology, and oncology, among others [36]. In the work by Zysk et al. [37], the investigators conducted a preliminary study to evaluate OCT as a tool to detect surgical margins in 3 patients. In this particular work, a computer-aided diagnostic algorithm was devised that classified the microanatomy images based on the fluctuations in image spatial frequency. The authors found that adipocytes, stroma, and tumor tissue exhibited identifiable differences in image spatial frequency, and were able to demonstrate that the technique could be useful for depth-resolved detection of residual cancer, down to 1.5 mm deep within the margin. Application of the technique to an independent test sample resulted in sensitivities ranging from 97–99% and specificities ranging from 56–68%. Although OCT confers the advantage of providing high resolution images of microanatomy (which could be analyzed by a trained observer, or by computer-aided techniques as the authors showed), the trade-off is that a single axial line scan in this case had a transverse resolution of 15 μm, making coverage of large areas of tissue potentially difficult. However, the development of lateral scanning or multiplexed systems could provide increased transverse tissue coverage while retaining the same depth coverage.

Our group has developed a contact-based quantitative diffuse reflectance imaging (Q-DRI) device which is capable of screening relatively large tissue areas with a well-defined sensing depth that satisfies the clinical criterion for tumor margin assessment [38]. The intra-operative margin studies in the breast carried out with this device will be the subject of the remainder of this article. The Q-DRI device consists of three components: an imaging probe, a console consisting of an optical imaging spectrometer and a computer with feature extraction software based on a fast, scalable Monte Carlo model. The hand-held imaging probe is placed in contact with the tissue to be measured. The remitted spectrally resolved signals or diffuse reflectance spectra are analyzed with the scalable Monte Carlo model [39,40] to reliably and quantitatively determine the wavelength dependent absorption and scattering coefficients of the tissue. The reduced scattering coefficient reflects the size and density of the scattering centers. The absorption coefficient is a linear combination of the product of the extinction coefficients and concentrations of constituent absorbers in tissue, i.e. β-carotene and hemoglobin. It has previously been shown by the Ramanujam group that the concentrations of β-carotene and hemoglobin and the reduced scattering coefficient are optical sources of contrast that show statistically significant differences between malignant and non-malignant breast tissues *ex vivo* [39,41–43]. The device is designed to be used on the excised tumor specimen (Fig. 3). The device is not designed or intended to replace

standard of care postoperative examination by a pathologist. All surgically resected samples which undergo evaluation with the device are always examined by the pathologist post-operatively.

Rationale for contact imaging

There are a number of previous publications that report on optical spectral imaging technologies for sub-surface tissue evaluation [44–46]. Most of these technologies relay the light to and from the tissue via non-contact optics coupled to a filtered broad band light source and CCD camera. The illumination and collection geometries are designed to maximize throughput and do not necessarily provide a well-defined sensing depth. Moreover, it is not possible to eliminate cross-talk between adjacent tissue pixels due to tissue scattering. Also, the spectral information obtained with these systems are generally displayed as intensity maps at a few discrete wavelengths and thus, do not fully exploit the spectral information content in the data and also, do not provide any quantitative molecular composition information underlying the measured diffuse reflectance intensities. Intra-operative margin assessment of breast tumors requires a sensing depth of 1–2 mm. This requires an imaging geometry that can be modeled to provide a well-defined sensing depth and one which can be accounted for in extraction of quantitative molecular information from the diffuse reflectance spectral measurements. The latter is important in providing quantitative endpoints that are independent of the instrument used, such that the underlying molecular composition can be compared across different instruments. The imaging geometry should also be designed to minimize cross-talk between adjacent channels. These attributes are most easily achieved through a contact, fiber based approach which is the basis for the design of our device.

Rationale for imaging for the excised tumor specimen

The approach described here is to image the boundaries of the excised tumor mass. There are a number of reasons why imaging of the tumor mass is desirable. The first is that this approach is consistent with the existing paradigm for postoperative pathologic margin assessment, which is important in designing clinical studies that have well-established clinical endpoints (in this case, post-operative pathologic assessment of the excised specimen). Another benefit is that it is more straightforward to design strategies to accurately co-register the margin-level images to margin-level pathology since they are both done on the excised mass. This is critical when validating a new technology. If the images are obtained *in vivo*, additional excisions would be needed for benchmarking the images against the gold standard, pathology, which would significantly alter standard of care. In addition, assessment of margins on the tumor mass obviates the need for the use of the device in a sterile field.

Comparison to intra-operative pathology

Table 2 contains a comparison of our spectral reflectance imaging device to currently available intra-operative pathology. The use of the device can be automated and thus does not require a pathologist on site. The device, in principle can cover the entire margin at a clinically relevant sensing depth (1–2 mm) of all breast tissue types including fatty tissues, thus providing full surveillance of breast tumor margins and it does not disrupt the tissue or interfere with post-operative pathology. The critical variable is the time that is needed to survey the margin in the intra-operative setting. The upper bound is set at 20–40 minutes, which is the time used to complete a frozen section or touch-prep analysis on the breast tissue. This is an important design constraint when developing a technology for intra-operative assessment of breast tumor margins. Our current device does not meet this requirement for the largest specimens, but prototypes are under development that will meet this requirement.

IV. Materials and Methods

A. Clinical study design

Margin assessment of the breast using our diffuse reflectance spectral imaging device was carried out on 57 eligible participants (women > 18 years of age) undergoing primary BCS for an invasive or non-invasive breast malignancy. The study was approved by the Institutional Review Board (IRB) at Duke University in accordance with assurances filed with and approved by the Department of Health and Human Services. A sub-group recruited to this study had undergone neo-adjuvant endocrine or chemotherapy prior to their surgical procedure. Operations were performed by 5 breast surgical oncologists at the Duke University Ambulatory Surgery Center. Each surgeon performed the lumpectomy according to their standard practice. The tissue was assessed grossly and via specimen mammography. The surgeons removed additional breast tissue based on their assessment of the margins. The surgeons did not perform routine immediate re-excision of each of the 6 margins. Frozen section and touch prep analyses were not performed on these specimens. Imaging of the resected tissue took place either in the operating room or an adjacent room, and commenced immediately following radiography of the specimen. On average, the imaging of the margin commenced within 18 ± 5 minutes of resection.

B. Hardware

A schematic of the optical spectral imaging instrument and multi-channel fiber optic probe is shown in Fig. 3. The instrument includes a 450 W Xenon Arc lamp, a monochromator (Gemini 180, J.Y. Horiba, Edison, NJ), an imaging spectrograph (Triax 320, JY HORIBA, Edison, NJ), and a CCD camera (Symphony, JY HORIBA, Edison, NJ). The monochromator and spectrograph are controlled using a GPIB interface (National Instruments, Austin, TX) and the CCD is controlled using an IP interface. The fixed parameters include the ruled plane gratings installed on the monochromator and spectrograph and the CCD pixel dimensions, which are instrument-specific and do not change throughout the duration of the study. The user can control all of the adjustable instrument parameters on the front panels of the LabVIEW programs described below.

A custom-designed, 8-channel fiber optic imaging probe (contract manufactured by RoMack Inc., Williamsburg, VA) is coupled to the imaging spectrometer. The 8 channels of the probe are held in place with an imaging plate and then interfaced with breast tissue specimens using an adjustable plexi-glass box. Each of the 8 probe channels is an individual fiber assembly with a core of 19 illumination fibers (200 μm, NA = 0.22) surrounded by 4 collection fibers (200 μm, NA = 0.22) (Fig. 3 – end view of the probe). Non-functional fibers are used to fill the dead space between the functional center fibers and the stainless steel jacket of the tip assembly. The typical power output at the probe tips is ~3 μW and 25 μW within a 10 nm band pass at 450 and 600 nm, respectively (the limits of the wavelength range used in clinical application of this device). At the illumination end, all 152 (19×8) illumination fibers are packed within dimensions of 6.615×1.715 mm at the exit slit of the monochromator. The entrance slit width at the imaging spectrograph is set to 1.2 mm and provides a spectral band pass of 3.17 nm using a 600 grooves/mm grating blazed at 400 nm. At the collection end of the fiber bundle, the 4 collection fibers from each channel are arranged vertically in 2×2 arrays, with each array separated vertically by two fiber spacings to minimize crosstalk between adjacent channels on the CCD. When coupled to the instrument, 8 diffuse reflectance spectra can be acquired simultaneously, one from each channel, by specifying these individual probe channel areas on the CCD using the LabVIEW program.

The components of the plexi-glass box and the fiber-optic imaging probe and box combination are shown in Fig. 4(a) and (b), respectively. The plexi-glass box holds the breast tissue specimen in place while it is being imaged and maintains the surgical orientation of each margin, enabling co-registration between the tissue composition maps derived from spectral imaging and pathological analysis. The plexi-glass box has a rectangular array of holes on each face with a diameter of 3.75 mm separated with a center-to-center distance of 5 mm and is adjustable in 1-dimension to conform to different sized partial mastectomy specimens. The probe tips of the 8 channels are arranged in a 4×2 array with 10 mm between each channel for placement in the plexi-glass box using an aluminum adaptor. A separation distance of 10 mm was chosen based on Monte Carlo simulations to minimize the crosstalk to <1% between adjacent channels.

C. Software Overview

LabVIEW (v 8.5.1, National Instruments, Austin, TX) is the main software platform used to communicate with the instrument components and control the data flow. A direct interface with Matlab (v 7.5.0, Mathworks, Natick, MA) is utilized to perform fast subroutines and data analysis using the fast, scalable Monte Carlo model [39]. The software package is designed to enable system calibration, data acquisition, real-time data display, data analysis, display of extracted optical parameter maps from the tissue margins, and display of extracted optical properties and constituent concentrations from individual locations on the tissue margin. The software also has built in quality control features to ensure that the spectra acquired meet the user's requirements (for instance, to automatically refine collection parameters to ensure the best signal to noise ratio (SNR), or to notify the user if any extracted parameters are outside of the expected range).

A unique feature of the custom software is that it is automatically setup to help the user keep track of probe placements within the specimen box during the scanning process. This is achieved via a visual diagram that represents one face of the plexi-glass box, and allows the user to collect data from the entire tissue surface by manual translation of the imaging probe, as described above. Once the tissue data acquisition process is complete, this is indicated by the user, and the software proceeds to analyze the data and display the results for the margin. The use of this software package in the clinic provides the user with the necessary tools for quantitative spectral imaging of tissue samples and rapid display of underlying tissue margin composition.

D. Phantom Validation and Sensing Depth Characterization

The imaging probe was validated for accuracy on a set of 36 tissue-simulating phantoms with optical properties covering the range observed by our group in the breast. The phantoms were composed of 1 μm polystyrene spheres as scatterers, and lyophilized human hemoglobin and the dye crocin (a water-soluble surrogate for β-carotene) as absorbers. The phantoms were prepared under atmospheric conditions, thus only the oxygenated form of hemoglobin was assumed to be present in the Monte Carlo inversion model. The average percent error in optical property extraction was 6.3% for the absorption coefficient and 9.81% for the mean reduced scattering coefficient. The errors in extraction for the parameters which approximated the most diagnostic parameters in the clinical study were 6.07% for oxy-hemoglobin:$< \mu_s' >$ and 11.76% for crocin:$< \mu_s' >$.

The sensing depth of the imaging probe was evaluated with Monte Carlo simulations employing the specific probe geometries and simulated for a range of tissue optical properties. Optical properties of pure adipose, fibroglandular, and malignant tissues extracted from pathology-confirmed pixels in the clinical study were used in the simulations. Single-layer and two-layer tissue geometries were simulated to approximate a wide variety

of tissue composition scenarios, for example, pure cancer (single-layer), or 1 mm of cancer below 1 mm of adipose (two-layer), in order to obtain a better understanding of the probe sensing depth for positive and close margins. For the single-layer model, the maximum sensing depth was for pure adipose tissue (0.7–2.2 mm over 450–600 nm), whereas the minimum was for pure cancer tissue (0.5–1.5 mm). For the two layer model (simulating a close margin), the maximum sensing depth was for adipose-cancer (0.7–1.7 mm) whereas the minimum was for fibroglandular-cancer (0.6–1.1 mm).

E. Data Acquisition, Calibration, Analysis and Display

To image a margin, the sample was placed in the plexi-glass container and the imaging probe was interfaced to the tissue through the holes in the container. At each pixel, 2 diffuse reflectance measurements spanning an overall range of 381–630 nm were collected. The imaging probe was manually translated horizontally and vertically by 5 mm, to sample inter-leaving holes between the 10 mm channel-to-channel spacing. In this manner, 2 successive placements of the probe sampled an area of 1.5 × 5.5 cm, with 5 mm transverse resolution, and required an average of 40 seconds for acquisition, analysis, and display. This process was repeated until the entire margin surface was sampled.

After margin imaging, the software allows the user to analyze and display the results. First all the saved tissue spectra and the saved calibration spectrum from the reflectance standard are normalized by the integration time used for each particular spectrum. The software then corrects the spectra at each pixel using a reflectance standard (Spectralon puck) measurement. The tissue spectra are sewn together the spectral regions covering 450–600 nm are sent into the fast, scalable Monte Carlo model for the extraction of optical properties and the underlying tissue composition. There is one additional scaling step prior to Monte Carlo analysis. Spectra from a breast tissue-mimicking phantom with known optical properties measured and saved on the computer are used to scale the Spectralon calibrated reflectance spectra prior to analysis with the fast, scalable Monte Carlo model [39,40]. The phantom spectra are also normalized by the reflectance standard (Spectralon puck) to account for day-to-day variations in throughput in the spectra collected from the phantom and the tissue (which are typically done on different days). This additional calibration step puts the experimental data and the simulated Monte Carlo data on the same scale.

The scalable Monte Carlo model extracts optical parameters including the wavelength-dependent absorption coefficient (μ_a) and the wavelength-dependent reduced scattering coefficient (μ_s') at each pixel (over the range 450–600 nm). The absorption coefficient is then used to calculate concentrations of oxy-hemoglobin, deoxyhemoglobin, total hemoglobin, and β-carotene, as well as the wavelength-averaged reduced scattering coefficient ($<\mu_s'>$). Parameter maps of the tumor margin can be created for any optical parameter extracted, and are user-selectable from the parameters listed above. For display, the maps were rendered using a 100× bicubic interpolation; however, for numerical data analysis, the raw image data were used.

F. Pathologic co-registration

Prior to optical spectral imaging, the specimen was marked with fiduciary markers placed by the surgeon, which orient the specimen anatomically (i.e., indicate which face is the superior margin, etc.) Using these orientation markers, margins of interest were selected (1 to 2 per specimen), and imaged by the research team using the Q-DRI instrument. Each margin per specimen that was imaged was then outlined using histological inks, to indicate the area imaged to the pathology department. The specimen was wrapped in gauze to prevent the inks from running, and sent to the pathology department using standard courier. The locations of the ink markers placed by the optical research team were noted by the pathology

assistants, and were used to define the margin boundaries for inking. In one case, the area imaged as a single margin by the optical team spanned multiple margins as assessed by the pathology assistants; in that case, the margin image data was eliminated from further consideration because of questionable co-registration. After further multi-color inking (a different colored ink for each margin) to preserve orientation, the specimen was then fixed in formalin overnight and subsequently "bread-loafed" into successive 3 mm thick transverse sections. From each of these 3 mm thick slices, a 5 μm section was cut and stained for pathologic analysis.

The margin-level diagnoses of the surgical margins of the primary surgical specimen were obtained from the postoperative pathology report. A key aspect of our study is that the margin images are reduced to scalar quantities, which are then paired with the margin-level diagnosis (positive, close, or negative) for classification. For the purposes of this study, margins that were classified by pathology as positive (cancer extending to the surface) or close (cancer within 2 mm of the surface) were classified as positive in our study, since the clinical implication for both positive and close margins is equivalent. The diagnosis of the margin for purposes of statistical analysis was determined by the type of residual carcinoma actually present at the margin, regardless of the type(s) of cancer present in the primary tumor. When the type of residual cancer at the margin was not specified by pathology, if only one type of cancer was present in the primary tumor then the margin was given the same diagnosis as the primary tumor. If multiple types of cancer were present in the primary tumor, no assumptions were made about the type of cancer present at the margin, and these margins were classified as "unspecified."

It must be noted that, because of the large specimen sizes, many tissues were not submitted in whole for pathologic evaluation and focal areas of malignancy may have been missed by pathology. In the ongoing clinical study, 28% of the specimens were processed in whole for histopathologic evaluation. In these cases, the whole surgical margin theoretically was visualized. However, practical limitations exist. Each paraffin block contains tissue that is ~3 mm thick. However, typically only one 5 μm section is cut and reviewed from each block. Thus, it is possible that small foci of margin involvement can be missed because the positive/close area may be in a different plane of section. The chance of missing a positive/close margin is higher in the 72% of lumpectomies that are not completely submitted. Only 20–50% of the margin is typically submitted for histologic processing in these cases, thus increasing the odds of missing grossly occult disease at or close to the specimen surface. While it certainly would be desirable to have detailed pathologic information at each pixel of our images, this is simply not practically possible given the size of the specimens. Because of the limited sampling done during pathologic assessment, the following criteria were used for including positive and negative margins for the development and testing off the classification algorithm. If positivity was found anywhere within the margin that was imaged, than it was clear that the margin was indeed positive. The problem was when the margin is found to be negative – in this case there could be potential for positive foci that were simply missed. Hence, only negative margins sampled from patients with all 6 margins determined as histologically negative were included as part of the negative margin cohort. Thus, the total number of margins evaluated in this study were 55 (34 positive and 21 negative) from 48 patients out of the 72 margins that were imaged in 57 patients. All of the negative margins included in the final analysis were from patients that had no positive margins elsewhere on the primary surgical specimen.

In addition to co-registering the imaged margins with margin-level histopathology as described above, specific pathologic analysis of certain pixels on each margin was obtained by random inking of 8–10 sites on the tissue by using a wooden dowel inserted through the holes in the specimen container. These inks were used by the pathologist to provide a more

detailed diagnosis of particular pixels on a margin. Due to the intensive nature of pathologic assessment, pathologic confirmation of individual pixels was only available for a small fraction (8–10 pixels) of any given margin.

V. Results and Discussion

An important feature of the Q-DRI device is the acquisition of maps of the specimen margins, reflective of a variety of biochemical and morphological sources of contrast in the breast. Sources of absorption contrast include hemoglobin (both oxygenated and deoxygenated forms) and β-carotene, whereas sources of scattering contrast include the size and density of scatterers within the tissue (e.g., varying number densities of subcellular organelles such as mitochondria, collagen content, and variations in the size of cell nuclei). These extracted parameters may be considered alone, or may be combined (for instance, by computing ratios) to further exploit diagnostic information. Although the Q-DRI device provides extracted parameter maps of the margin with spatial information intact, traditional image analysis is difficult because there is no prior information about the spatial characteristics of positive and close margins to leverage upon. Thus, it is necessary to devise strategies for reducing the image data into substitute variables which can best predict margin status.

One approach to image reduction we have pursued is computation of descriptive statistical variables which capture important features of the margin images. These include, but are not limited to, the mean, maximum, minimum, or variance of the values in a particular extracted parameter image. Another successful approach is to analyze the distribution of values within a particular image, for which histograms are useful tools. For example, by plotting histograms for each margin parameter image, natural distinctions between positive and negative margins may be observed in the distribution of the image values. A number of parameters including, total hemoglobin concentration, β-carotene concentration, $<\mu_s'>$, hemoglobin saturation, oxy-hemoglobin concentration, deoxy-hemoglobin concentration, and the ratios of various combinations of these parameters, were evaluated.

Fig. 5 contains representative maps of two such parameters: the ratio of β-carotene:$< \mu_s'>$ (left image) as well as the ratio of total hemoglobin:$< \mu_s'>$ (right image), and the corresponding histograms which graphically represent the distribution of values within each image for a margin negative for residual disease. Fig. 6 contains representative images of the same parameters in a margin positive for invasive ductal carcinoma (IDC). These figures are full screenshots taken from the custom software application. β-carotene is a dietary carotenoid known to be stored primarily in adipocytes, and is thus reflective of the amount of fat present in the sensing volume. The wavelength-averaged reduced scattering coefficient, $<\mu_s'>$, is a measure of the amount of light elastically scattered in the tissue, with higher scattering coefficients associated with more connective tissue and denser arrangements of cells and their subcellular scatterers such as organelles and membranes (scatter density) as well as with changes in the distribution of sizes of these scatterers (scatter size) [47].

Additionally, the extracted total hemoglobin concentration is reflective of the vascular volume present within the sensing volume of the Q-DRI device. (Separate studies have shown that this parameter is stable with respect to time following tissue removal, as described later). It is well known that angiogenesis, or creation of new blood vessels, is a hallmark of cancer. Thus, increased levels of total hemoglobin could be reflective of angiogenic processes in the tissue and thus indicative of cancer.

As observed in Fig. 7, positive margins were hallmarked by decreased levels in both β-carotene:$< \mu_s' >$ as well as total hemoglobin:$< \mu_s' >$. Therefore, in Figs. 5 and 6, the colormaps are set such that lower values of β-carotene:$< \mu_s' >$ and total hemoglobin:$< \mu_s' >$ appear red, whereas higher values appear blue. As seen in the images, the negative margin images (Fig. 5) are characterized by a higher proportion of blue pixels, whereas the positive margin images (Fig. 6) are characterized by increased proportions of red pixels, for both parameters of interest. The black circles in the images of Fig. 6 indicate the locations of path-confirmed cancerous pixels, and the white circles indicate the locations of normal pixels, which confirm these generalizations. Analysis of these path-confirmed pixels suggests that the most specific contrast appears to be contained in the β-carotene:$< \mu_s' >$ images.

It must be noted, that breast tissue is highly heterogeneous, and it is difficult to isolate one or two unique parameters in our data which contain all of the diagnostic information. However, based on a separate analysis of path-confirmed pixels, we suspect that the primary value of dividing β-carotene and total hemoglobin by $<\mu_s'>$ is to normalize for differences in highly scattering collagen content (i.e. breast density) between patients. However, $<\mu_s'>$ is also associated with malignancy and is expected to provide additional diagnostic information in addition to β-carotene and total hemoglobin concentration. Thus, normalization by $<\mu_s'>$ could change the expected trends, since both numerator and denominator are affected by malignancy.

The percentage of pixels below a particular threshold for β-carotene:$< \mu_s' >$ and total hemoglobin:$< \beta_s' >$ exhibited the greatest differences between positive and negative margins in this dataset, as determined by Wilcoxon rank-sum testing. The following text describes how the optimal threshold was selected for each of the above two parameters in order to build predictors for margin-level assessment from the parameter maps. A threshold value for pixel intensity was determined and the percentage of pixels below that threshold was computed. A Wilcoxon Rank Sum test was carried out to determine if the percentage of pixels below that threshold was statistically different between positive and negative margins. The optimal threshold was determined by repeating the Wilcoxon tests across the full range of threshold values, the results of which showed that 6 μM-cm for β-carotene:$< \mu_s' >$ showed the greatest degree of association with pathology ($p < 0.002$). A similar process was applied to total hemoglobin:$< \mu_s' >$, such that the percentage of pixels below a threshold value of 8 μM-cm resulted in the statistically most significant differences between positive and negative margins for that parameter ($p < 0.01$). Fig. 7 contains boxplots that graphically demonstrate these differences.

Using the feature extraction algorithm described by Wilke et al. [38] and summarized below, the program then determines a margin-level diagnosis for the imaged tissue. A tree-based approach was taken to build the two-parameter model, such that a margin was classified as positive if the percentage of image pixels for the β-carotene:$< \mu_s' >$ OR total hemoglobin:$< \mu_s' >$ parameters were above their respective thresholds; otherwise it was classified as negative. These percentages were each varied across the complete set of different threshold values from 0–100%, and the sensitivity and specificity was then calculated against margin-level histopathology. The optimal pair of threshold values was determined by a receiver operator characteristic analysis and the Youden index, in order to maximize the sensitivity and specificity in an additive manner. The average optimal pair of threshold values in the final cross-validated model for β-carotene:$< \mu_s' >$ and total hemoglobin:$< \mu_s' >$ were 98 ± 0.19 % and 72 ± 1.0 %, respectively. The percentage of pixels below 6 μM-cm for β-carotene:$< \mu_s' >$ and below 8 μM-cm for total hemoglobin:$< \mu_s' >$ is displayed within each respective histogram in Figs. 5 and 6, and the overall margin diagnosis is displayed using this algorithm. With a leave-one-out cross validation technique (an alternative to prospective

testing in the absence of a large sample size), an unbiased estimate of 80% sensitivity and 67% specificity was achieved. Of the 55 margins, 41 were correctly identified by the algorithm.

Table 3 contains a summary of the overall classification performance of the device, as well as the performance of the device in detecting disease as a function of depth from the surface. For this analysis, the positive margins were subdivided into four categories: 1) truly positive margins, with cancer extending to the surface, 2) close margins, with cancer within 1 mm of the surface, 3) close margins, with cancer between 1–2 mm of the margin surface, and 4) margins which were diagnosed as containing cancer within 2 mm of the surface, but in which the exact distance was not specified and is therefore unknown (could be in either of categories 1–3).

The results indicate that the device was more accurate in detecting cancer at the surface than in detecting cancer within 1 mm of the margin, which is not unexpected given the average sensing depth noted previously. Interestingly, however, the accuracy of detecting close margins between 1–2 mm of the margin surface exceeded that of close margins within 1 mm of the surface. It should be noted that the majority of the positive margins in this study were truly positive (17), and there were only 7 margins close within 1 mm, and 6 margins close between 1–2 mm. Because the disease variant was not considered in this depth-wise analysis, it is possible that the results were biased by an uneven distribution of disease variants across the depth categories. Specifically, of the 7 margins close within 1 mm, the 2 misdiagnosed margins contained DCIS and mixed IDC/DCIS, respectively. Conversely, in the close between 1–2 mm category, of the 6 margins, only 1 margin (containing IDC) was misdiagnosed. However, the significance of the cancer type on the difference in depth-wise accuracy is not clear because of the small sample sizes and the fact that the two categories differ by only one missed margin. Table 4 presents the performance of the device in classifying positive or close margins as a function of disease type found at the margin. Interestingly, the device correctly identified 8 of 9 margins positive for ductal carcinoma *in situ* (DCIS) which corresponds to a sensitivity of 89%. Detection of DCIS intraoperatively is particularly important, since DCIS presents a challenge for surgeons due to its low mammographic density (making it difficult or impossible to see in specimen radiographs), as well as its indistinct gross characteristics.

One consideration in any study concerned with examination of excised tissue is potential degradation (or temporal change) of the tissue or its associated optical properties. To address this question, degradation studies have been performed on freshly excised tissues to assess the effect of time after excision on the predictive features used to identify positive tumor margins with this technology. It was found that within a 30-minute window (the time frame over which intra-operative margin assessment would occur), time after excision has comparable effects on the optical contrast between positive and negative tumor margins, as compared to the error in the measurement established by taking multiple measurements of the same tissue by removing and replacing the probe. Specifically, the coefficient of variation due to temporal effects in 13 tumor tissues was 0.07 ± 0.03 and 0.21 ± 0.21 for β-carotene:$< \mu_s' >$ and total hemoglobin:$< \mu_s' >$, respectively, whereas in 15 benign tissues the coefficients of variation of the same variables were 0.23 ± 0.48 and 0.17 ± 0.21. Conversely, in the reproducibility study, the coefficient of variation in 32 measurements from a 4 benign samples was 0.08 ± 0.05 and 0.11 ± 0.11 for β-carotene:$< \mu_s' >$ and total hemoglobin:$< \mu_s' >$, respectively.

VI. Conclusions and Future Work

For optical spectral imaging to be used routinely in the clinic as a diagnostic tool, an accurate, robust and reliable instrument and probe design is critical. To consistently yield accurate estimation of tissue optical properties, calibration is required to compensate for lamp intensity fluctuations, wavelength-dependent instrument response, inter-device variations, and fiber bending losses during the measurement [48,49]. Current calibration techniques typically rely on measurements using power meters, reflectance standards, and/or tissue phantoms, typically before or after the clinical measurements are completed [42,50–53]. There are a number of limitations associated with such calibration methods. First, because the calibration is performed at the beginning or end of the study, real-time instrument fluctuations, such as lamp drift and fiber bending loss can not be compensated for by these calibration approaches. Second, they can require an additional 30 minutes for lamp warm up and another 10–20 minutes for calibration, which is a significant problem in a clinical setting such as the operating room. Our group has recently reported a novel fiber optic probe with self-calibration capability for performing UV-VIS DRS [54]. The probe has a built-in calibration channel that can be used to record the lamp spectrum and instrument/fiber responses concurrently with tissue measurements. The self-calibrating probe with a new calibration procedure can effectively correct for instrument and probe responses, short- and long-term lamp fluctuations, and fiber bending loss. Most importantly, it removes the need of instrument warm-up and additional calibration measurements in the clinic, therefore saving 40–60 minutes of precious clinical time.

Specifically for intra-operative assessment of tumor margins, fast imaging speed and wide margin coverage is also a key for the success of optical spectroscopy in the OR. Due to stringent time constraints in the intra-operative setting and to minimize systematic errors (sample degradation) that may influence *ex vivo* tissue imaging, the spectroscopic device needs to image all 6 margins of an excised tumor mass within 30 minutes, i.e. within 5 minutes per margin. The size of the largest margin seen in the specimens that have been imaged thus far in the clinical study at Duke is up to 4.5 cm × 9.5 cm (~40 cm^2, Fig. 2). This makes it not feasible to survey a single large size margin with reasonable resolution using a single-point probe.

Bench-top spectral imaging devices currently used in clinical studies by various research groups including the one described in this article typically consist of a broad band light source for illumination, an imaging spectrograph and CCD for detection and an imaging fiber bundle for delivery to and collection of light from the tissue [50,55]. This technology is an excellent tool for proof-of-concept studies but is less practical for an intra-operative setting where time, cost and space are at a premium. Thus a simpler, low-cost, more portable reflectance spectral imaging system, capable of making fast measurements at multiple sites rapidly is desired during clinical studies [56]. Therefore, a miniature spectral imaging system that utilizes the same scientific principles as the bench-top system, but hurdles technical issues including complexity, cost and size in order to make this technology clinically translatable for tumor margin assessment is desired. Fortunately, the rapid advancement of optoelectronics in the past decades makes the construction of a miniature spectral imaging system possible using high power light emitting diodes (LEDs) and low noise photodiodes (PDs). We envision that a next generation margin assessment device would be an integration of multiple high power LEDs as light source, light delivery network and an array of PDs that can be brought in direct contact with tissue. As a proof of concept, we have recently developed a miniature single-pixel device in which the detection fiber bundle and spectrometer of the bench-top system was replaced by a photodiode [57,58]. We demonstrated that the modified device is capable of extracting optical properties in tissue phantoms with good accuracy in the 400–600 nm range comparable to the clinical benchtop

system. Furthermore, the results from the wavelength reduction simulations from the measured phantom data show that it is possible to replace the lamp and monochromator with several high powered LEDs in the 400–600 nm range for higher throughput, smaller size, and much lower cost. By strategically choosing high powered LEDs with a 20–30 nm bandwidth while covering most of the 400–600 nm range, an LED-photodiode device can be created and used to extract a similar range of tissue optical properties.

The number of new and innovative optical solutions to the problem of tumor margin assessment, as covered in this article, provides promise that incomplete primary tumor resections could become a phenomenon of the past. The use of our Q-DRI device on a cohort of 55 margins from 48 patients indicated that this technology is helpful in discriminating positive from negative margins in the intra-operative setting. Continued refinements to the device should result in a clinically-practical device with potential for widespread clinical application.

Acknowledgments

This publication was made possible by Grant Number 1UL1 RR024128-01 from the National Center for Research Resources (NCRR), a component of the National Institutes of Health (NIH), and NIH Roadmap for Medical Research. Its contents are solely the responsibility of the authors and do not necessarily represent the official view of NCRR or NIH. J. Q. Brown acknowledges NRSA support from the NCI, F32CA124058.

References

1. SUROS News Release. New Method for Breast Cancer Diagnosis. 2003.
2. Tartter PI, Kaplan J, Bleiweiss I, Gajdos C, Kong A, Ahmed S, Zapetti D. Lumpectomy margins, reexcision, and local recurrence of breast cancer. Am J Surg. Feb.2000 179:81–5. [PubMed: 10773138]
3. Kunos C, Latson L, Overmoyer B, Silverman P, Shenk R, Kinsella T, Lyons J. Breast conservation surgery achieving >or=2 mm tumor-free margins results in decreased local-regional recurrence rates. Breast J. Jan-Feb.2006 12:28–36. [PubMed: 16409584]
4. Elkhuizen PH, van de Vijver MJ, Hermans J, Zonderland HM, van de Velde CJ, Leer JW. Local recurrence after breast-conserving therapy for invasive breast cancer: high incidence in young patients and association with poor survival. Int J Radiat Oncol Biol Phys. Mar 1.1998 40:859–67. [PubMed: 9531371]
5. Balch GC, Mithani SK, Simpson JF, Kelley MC. Accuracy of intraoperative gross examination of surgical margin status in women undergoing partial mastectomy for breast malignancy. Am Surg. Jan.2005 71:22–7. discussion 27–8. [PubMed: 15757052]
6. Dillon MF, Mc Dermott EW, O'Doherty A, Quinn CM, Hill AD, O'Higgins N. Factors affecting successful breast conservation for ductal carcinoma in situ. Ann Surg Oncol. May.2007 14:1618–28. [PubMed: 17443388]
7. Fleming FJ, Hill AD, Mc Dermott EW, O'Doherty A, O'Higgins NJ, Quinn CM. Intraoperative margin assessment and re-excision rate in breast conserving surgery. Eur J Surg Oncol. Apr.2004 30:233–7. [PubMed: 15028301]
8. Huston TL, Pigalarga R, Osborne MP, Tousimis E. The influence of additional surgical margins on the total specimen volume excised and the reoperative rate after breast-conserving surgery. Am J Surg. Oct.2006 192:509–12. [PubMed: 16978962]
9. Jacobs L. Positive margins: the challenge continues for breast surgeons. Ann Surg Oncol. May.2008 15:1271–2. [PubMed: 18320287]
10. Kotwall C, Ranson M, Stiles A, Hamann MS. Relationship between initial margin status for invasive breast cancer and residual carcinoma after re-excision. Am Surg. Apr.2007 73:337–43. [PubMed: 17439024]
11. Mendez JE, Lamorte WW, de Las Morenas A, Cerda S, Pistey R, King T, Kavanah M, Hirsch E, Stone MD. Influence of breast cancer margin assessment method on the rates of positive margins and residual carcinoma. Am J Surg. Oct.2006 192:538–40. [PubMed: 16978970]

12. Menes TS, Tartter PI, Mizrachi H, Smith SR, Estabrook A. Touch preparation or frozen section for intraoperative detection of sentinel lymph node metastases from breast cancer. Ann Surg Oncol. Dec.2003 10:1166–70. [PubMed: 14654472]
13. Smitt MC, Nowels KW, Zdeblick MJ, Jeffrey S, Carlson RW, Stockdale FE, Goffinet DR. The importance of the lumpectomy surgical margin status in long-term results of breast conservation. Cancer. Jul 15.1995 76:259–67. [PubMed: 8625101]
14. Waljee JF, Hu ES, Newman LA, Alderman AK. Predictors of re-excision among women undergoing breast-conserving surgery for cancer. Ann Surg Oncol. May.2008 15:1297–303. [PubMed: 18259820]
15. Cox CE, Ku NN, Reintgen DS, Greenberg HM, Nicosia SV, Wangensteen S. Touch preparation cytology of breast lumpectomy margins with histologic correlation. Arch Surg. Apr.1991 126:490–3. [PubMed: 2009065]
16. Cox CE, Hyacinthe M, Gonzalez RJ, Lyman G, Reintgen D, Ku NN, Miller MS, Greenberg H, Nicosia SV. Cytologic evaluation of lumpectomy margins in patients with ductal carcinoma in situ: clinical outcome. Ann Surg Oncol. Dec.1997 4:644–9. [PubMed: 9416412]
17. Chagpar A, Yen T, Sahin A, Hunt KK, Whitman GJ, Ames FC, Ross MI, Meric-Bernstam F, Babiera GV, Singletary SE, Kuerer HM. Intraoperative margin assessment reduces reexcision rates in patients with ductal carcinoma in situ treated with breast-conserving surgery. Am J Surg. Oct. 2003 186:371–7. [PubMed: 14553853]
18. Cendan JC, Coco D, Copeland EM 3rd. Accuracy of intraoperative frozen-section analysis of breast cancer lumpectomy-bed margins. J Am Coll Surg. Aug.2005 201:194–8. [PubMed: 16038815]
19. Camp ER, McAuliffe PF, Gilroy JS, Morris CG, Lind DS, Mendenhall NP, Copeland EM 3rd. Minimizing local recurrence after breast conserving therapy using intraoperative shaved margins to determine pathologic tumor clearance. J Am Coll Surg. Dec.2005 201:855–61. [PubMed: 16310688]
20. Taroni P, Pifferi A, Torricelli A, Comelli D, Cubeddu R. In vivo absorption and scattering spectroscopy of biological tissues. Photochem Photobiol Sci. Feb.2003 2:124–9. [PubMed: 12664972]
21. Bigio IJ, Brown SG, Briggs G, Kelley C, Lakhani S, Picard D, Ripley PM, Rose IG, Saunders C. Diagnosis of breast cancer using elastic-scattering spectroscopy: preliminary clinical results. Journal of Biomedical Optics. 2000; 5:221–228. [PubMed: 10938787]
22. Welch, AJ.; Gemert, MJCV. Optical-thermal response of laser-irradiated tissue. New York: Plenum Press; 1995.
23. Bigio I, Mourant J. Ultraviolet and visible spectroscopies for tissue diagnostics: fluorescence spectroscopy and elastic-scattering spectroscopy. Physics in Medicine and Biology. 1997; 42:803–814. [PubMed: 9172260]
24. Zuzak KJ, Schaeberle MD, Gladwin MT, Cannon RO 3rd, Levin IW. Noninvasive determination of spatially resolved and time-resolved tissue perfusion in humans during nitric oxide inhibition and inhalation by use of a visible-reflectance hyperspectral imaging technique. Circulation. Dec 11.2001 104:2905–10. [PubMed: 11739304]
25. Srinivasan S, Pogue BW, Jiang S, Dehghani H, Kogel C, Soho S, Gibson JJ, Tosteson TD, Poplack SP, Paulsen KD. Interpreting hemoglobin and water concentration, oxygen saturation, and scattering measured in vivo by near-infrared breast tomography. PNAS. 2003; 100:12349–54. [PubMed: 14514888]
26. Bigio IJ, Bown SG, Briggs G, Kelley C, Lakhani S, Pickard D, Ripley PM, Rose IG, Saunders C. Diagnosis of breast cancer using elastic-scattering spectroscopy: preliminary clinical results. J Biomed Opt. Apr.2000 5:221–8. [PubMed: 10938787]
27. Bohren, CF.; Huffman, DA. Absorption and Scattering of Light by Small Particles. New York: John Wiley & Sons; 1983.
28. Haka AS, Volynskaya Z, Gardecki JA, Nazemi J, Lyons J, Hicks D, Fitzmaurice M, Dasari RR, Crowe JP, Feld MS. In vivo margin assessment during partial mastectomy breast surgery using raman spectroscopy. Cancer Res. Mar 15.2006 66:3317–22. [PubMed: 16540686]

29. Frank CJ, Mccreery RL, Redd DCB. Raman-Spectroscopy of Normal and Diseased Human Breast Tissues. Analytical Chemistry. Mar 1.1995 67:777–783. [PubMed: 7762814]
30. Haka AS, Shafer-Peltier KE, Fitzmaurice M, Crowe J, Dasari RR, Feld MS. Diagnosing breast cancer by using Raman spectroscopy. Proceedings of the National Academy of Sciences of the United States of America. Aug 30.2005 102:12371–12376. [PubMed: 16116095]
31. Marzullo ACD, Neto OP, Bitar RA, Martinho HD, Martin AA. FT-Raman spectra of the border of infiltrating ductal carcinoma lesions. Photomedicine and Laser Surgery. Oct.2007 25:455–460. [PubMed: 17975961]
32. Keller MD, Majumder SK, Mahadevan-Lansen A. Spatially offset Raman spectroscopy of layered soft tissues. Optics Letters. Apr 1.2009 34:926–928. [PubMed: 19340173]
33. Bouma, BE.; Tearney, GJ. Handbook of Optical Coherence Tomography. Marcel Dekker Inc; 2001.
34. Schmitt JM. Optical coherence tomography (OCT): a review. IEEE journal of selected topics in quantum electronics. 1999; 5:1205–1215.
35. Fercher AF, Drexler W, Hitzenberger CK, Lasser T. Optical coherence tomography - principles and applications. Rep Prog Phys. 2003; 66:239–303.
36. Zysk AM, Nguyen FT, Oldenburg AL, Marks DL, Boppart SA. Optical coherence tomography: a review of clinical development from bench to bedside. J Biomed Opt. Sep-Oct.2007 12:051403. [PubMed: 17994864]
37. Zysk AM, Boppart SA. Computational methods for analysis of human breast tumor tissue in optical coherence tomography images. J Biomed Opt. Sep-Oct.2006 11:054015. [PubMed: 17092164]
38. Wilke LG, et al. Rapid Non-invasive Imaging of Tissue Composition in Breast Tumor Margins. ASBS, American Journal of Surgery. 2009 (Accepted).
39. Palmer GM, Ramanujam N. A Monte Carlo-based inverse model for calculating tissue optical properties. Part I: Theory and validation on synthetic phantoms. Appl Opt. Feb 10.2006 45:1062–71. [PubMed: 16512550]
40. Palmer GM, Zhu C, Breslin TM, Xu F, Gilchrist KW, Ramanujam N. A Monte Carlo-based inverse model for calculating tissue optical properties. Part II: Application to breast cancer diagnosis. Appl Opt. Feb 10.2006 45:1072–8. [PubMed: 16512551]
41. Zhu C, Palmer GM, Breslin TM, Harter J, Ramanujam N. Diagnosis of breast cancer using fluorescence and diffuse reflectance spectroscopy: a Monte-Carlo-model-based approach. J Biomed Opt. May-Jun.2008 13:034015. [PubMed: 18601560]
42. Zhu C, Palmer GM, Breslin TM, Harter J, Ramanujam N. Diagnosis of breast cancer using diffuse reflectance spectroscopy: Comparison of a Monte Carlo versus partial least squares analysis based feature extraction technique. Lasers Surg Med. Aug.2006 38:714–24. [PubMed: 16799981]
43. Palmer GM, Zhu CF, Breslin TM, Xu FS, Gilchrist KW, Ramanujam N. Monte Carlo-based inverse model for calculating tissue optical properties. Part II: Application to breast cancer diagnosis. Applied Optics. Feb 10.2006 45:1072–1078. [PubMed: 16512551]
44. Utzinger U, Richards-Kortum RR. Fiber optic probes for biomedical optical spectroscopy. J Biomed Opt. Jan.2003 8:121–47. [PubMed: 12542388]
45. McLain BL, Ma Jiaying, Ben-Amotz Dor. Optical Absorption and Fluorescence Spectral Imaging Using Fiber Bundle Image Compression. Applied Spectroscopy. 1999; 53:1118–1122.
46. Gebhart SC, Thompson RC, Mahadevan-Jansen A. Liquid-crystal tunable filter spectral imaging for brain tumor demarcation. Appl Opt. Apr 1.2007 46:1896–910. [PubMed: 17356636]
47. Mourant JR, Freyer JP, Hielscher AH, Eick AA, Shen D, Johnson TM. Mechanisms of light scattering from biological cells relevant to noninvasive optical-tissue diagnostics. Applied Optics. Jun 1.1998 37:3586–3593. [PubMed: 18273328]
48. Nichols MG, Hull EL, Foster TH. Design and testing of a white-light, steady-state diffuse reflectance spectrometer for determination of optical properties of highly scattering systems. Appl Opt. Jan 1.1997 36:93–104. [PubMed: 18250650]
49. Marin NM, MacKinnon N, MacAulay C, Chang SK, Cox D, Serachitopol D, Pikkula B, Follen M, Richards-Kortum R. Calibration standards for multicenter clinical trials of fluorescence spectroscopy for in vivo diagnosis. J Biomed Opt. 2006; 11:014010. [PubMed: 16526887]

50. Utzinger U, Brewer M, Silva E, Gershenson D, Blast RC Jr, Follen M, Richards-Kortum R. Reflectance spectroscopy for in vivo characterization of ovarian tissue. Lasers Surg Med. 2001; 28:56–66. [PubMed: 11430444]

51. Zonios G, Perelman LT, Backman V, Manoharan R, Fitzmaurice M, Van Dam J, Feld MS. Diffuse reflectance spectroscopy of human adenomatous colon polyps in vivo. Appl Opt. Nov 1.1999 38:6628–37. [PubMed: 18324198]

52. Mirabal YN, Chang SK, Atkinson EN, Malpica A, Follen M, Richards-Kortum R. Reflectance spectroscopy for in vivo detection of cervical precancer. J Biomed Opt. Oct.2002 7:587–94. [PubMed: 12421125]

53. Thueler P, Charvet I, Bevilacqua F, St Ghislain M, Ory G, Marquet P, Meda P, Vermeulen B, Depeursinge C. In vivo endoscopic tissue diagnostics based on spectroscopic absorption, scattering, and phase function properties. J Biomed Opt. Jul.2003 8:495–503. [PubMed: 12880356]

54. Yu B, Fu H, Bydlon T, Bender JE, Ramanujam N. Diffuse reflectance spectroscopy with a self-calibrating fiber optic probe. Opt Lett. 2008; 33:1783–85. [PubMed: 18709086]

55. Nichols MG, Hull EL, Foster TH. Design and testing of a white-light, steady-state diffuse reflectance spectrometer for determination of optical properties of highly scattering systems. Appl Opt. 1997; 36:93–104. [PubMed: 18250650]

56. Feather JW, Ellis DJ, Leslie G. A portable reflectometer for the rapid quantification of cutaneous haemoglobin and melanin. Phys Med Biol. Jun.1988 33:711–22. [PubMed: 3406055]

57. Yu B, Lo JY, Kuech TF, Palmer GM, Bender JE, Ramanujam N. Cost-effective diffuse reflectance spectroscopy device for quantifying tissue absorption and scattering in vivo. Journal of Biomedical Optics Letters. 2008; 13:060505.

58. Lo JY, Yu B, Fu HL, Bender JE, Palmer GM, Kuech TF, Ramanujam N. A strategy for quantitative spectral imaging of tissue absorption and scattering using light emitting diodes and photodiodes. Opt Express. Feb 2.2009 17:1372–84. [PubMed: 19188966]

Biographies

J. Quincy Brown (S ‘01, M ‘05) received the B.S. degree (2001) and the Ph.D. degree (2005) in biomedical engineering from Louisiana Tech University. Dr. Brown is currently an NIH NRSA Postdoctoral Fellow at Duke University, where his research interests include development and clinical validation of spectroscopic tools for cancer diagnosis, prognosis, and therapeutic monitoring, and optical molecular imaging for basic science and preclinical cancer applications.

Torre M. Bydlon received a B.S. degree in Electrical Engineering from Tufts University in 2006 with a second major in Biomedical Engineering. Torre is a Department of Defense Breast Cancer Research Program Predoctoral Trainee and is currently researching the use of optical spectroscopic imaging for breast tumor margin assessment.

Lisa Richards received her B.S.E. degree in Biomedical Engineering from Duke University in 2008. She continued in the lab through the summer of 2009 as an Associate in Research and was focused on the development of software to enable real-time intraoperative breast tumor margin assessment using optical spectroscopy.

Bing Yu received B.S. and M.S. degrees in Optoelectronics Technology from University of Electronic Science and Technology of China UESTC) in 1989 and 1994, respectively, and a Ph.D. in Electrical Engineering from Virginia Tech in 2005. He is currently a Senior Research Scientist in the Biomedical Engineering Department at Duke University. His current research interests include tissue optics, optical spectroscopy and imaging for cancer diagnostics, fiber optic sensors, and optical instrumentation.

Stephanie A. Kennedy received a Bachelor of Biomedical Engineering (2006) from the Catholic University of America. She is currently pursuing a Ph.D. in Biomedical Engineering Duke University. Her research interests include development of intra-operative tools and predictive models for spectroscopic analysis and diagnosis of breast cancer margins.

Joseph Geradts is a surgical pathologist with special expertise in diseases of the breast, and has been Professor of Pathology at Duke University Medical Center since 2005. Dr. Geradts received an M.A. in Endocrinology from the University of California, Berkeley, CA, and the M.D. from the University of Chicago. Dr. Geradts completed his residency in anatomic pathology at the University of California, San Francisco, and a fellowship in Surgical Pathology at Stanford University Medical Center, before serving as a Postdoctoral Fellow at the National Cancer Institute. Dr. Geradts' research interests include identifying genetic markers of early breast cancer progression, and the use of optical imaging for directed sampling of breast tumor margins.

Lee G. Wilke is an Associate Professor of Surgery at the Duke University Medical Center. She graduated Magna Cum Laude from Duke University in 1989 with a degree in Neurosciences. Dr. Wilke received a Howard Hughes Research Fellowship while in medical school, and in 1993, she completed her M.D. at Duke University. From 1993 to 2000, Dr Wilke attended the University of Michigan for her surgical residency. Dr Wilke is currently completing a Masters of Clinical Research at Duke University and remains active in breast cancer clinical trials and translational research.

Marlee K. Junker is a Research Analyst in Dr. Nimmi Ramanujam's laboratory at Duke University's Department of Biomedical Engineering. Marlee received her B.S. degree summa cum laude in Biology (2004) and her M.S. degree in Molecular and Cellular Biology (2006) from the University of Massachusetts, Amherst.

Jennifer Gallagher is with the Duke Clinical Research Unit of the Duke University Medical Center.

William T. Barry is an Assistant Professor of Biostatistics and Bioinformatics at the Duke University Medical Center, with experience in the design and analysis of laboratory experiments and clinical trials related to breast cancer research. Dr. Barry received his Ph.D. in Biostatistics from the University of North Carolina at Chapel Hill, and currently serves as the Director of Bioinformatics for the Duke Comprehensive Cancer Center. Dr Barry is a Statistician for Cancer and Leukemia Group B and a member of the Clinical Genomics Studies Unit at the Duke Institute for Genome Science and Policy (IGSP).

Nimmi Ramanujam is Associate Professor of BME at Duke University and the Director of the Tissue Optical Spectroscopy Laboratory (TOpS Lab) in the Pratt School of Engineering at Duke University. The lab specializes in the development of optical systems for the clinical detection of cancer and mathematical algorithms for quantitative physiology of cancers *in vivo*. Her current research program focuses on developing light based technologies for breast cancer. She has over 16 years experience in optical spectroscopy, modeling light-tissue interaction, and translational research and has authored over 50 peer-reviewed journal articles, 6 book chapters and 10 patents. Dr. Ramanujam was named by MIT's prestigious Technology Review as one of the top 100 young innovators in technology in 2003, named a DOD Era of Hope Scholar for Breast Cancer research in 2004 and won the Global Indus Technovators award from MIT in 2005. Dr. Ramanujam has a Ph.D. in Biomedical Engineering and a M.S. in Mechanical Engineering from the University of Texas, Austin.

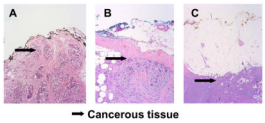

Fig. 1.

Photomicrographs of H&E-stained breast tumor margin sections, representative of (A) invasive ductal carcinoma extending the full length of the margin (positive) (B) at ~1mm from the surgical margin (close) and (B) greater than 2 mm from the inked surface (negative).

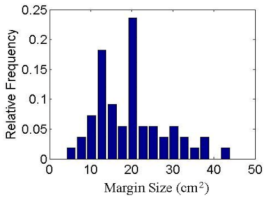

Fig. 2.
Distribution of single margin areas observed in 120 BCS patients.

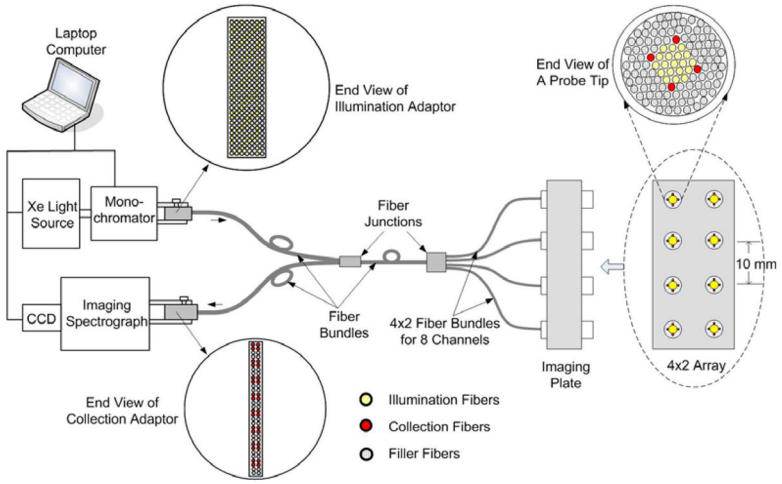

Fig. 3.

Schematic of the clinical instrument and the fiber arrangement of the multi-channel probe. Each channel has 4 (200 μm) collection fibers and a central bundle of 19 (200 μm) illumination fibers. All 8 channels are arranged in a 4×2 array with a separation distance of 10 mm (center to center).

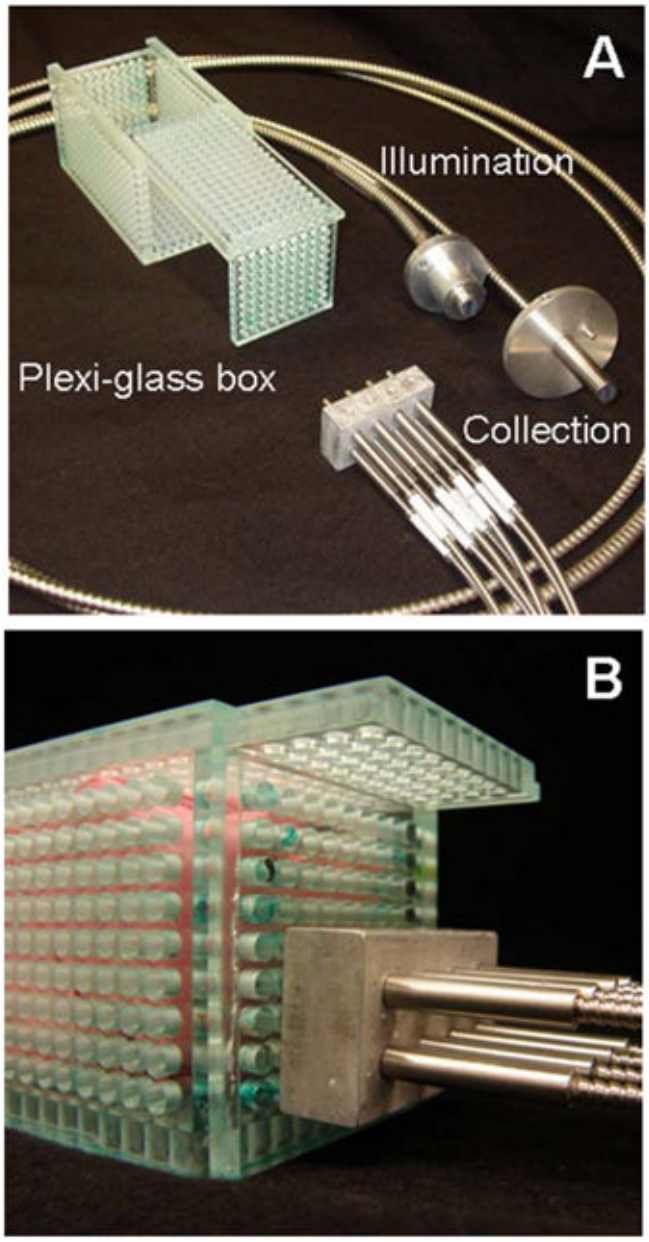

Fig. 4.

A) Photograph of the multi-channel fiber optic probe in an aluminum adaptor to space each of the 8 probes 10 mm apart in a 2 × 4 configuration, and the two pieces of the plexi-glass box, B) Photograph of a mockup of a lumpectomy specimen being imaged in the plexi-glass box. The two pieces of the box slide together to hold the specimen in place and the probe is placed in contact with the specimen via the holes in the box.

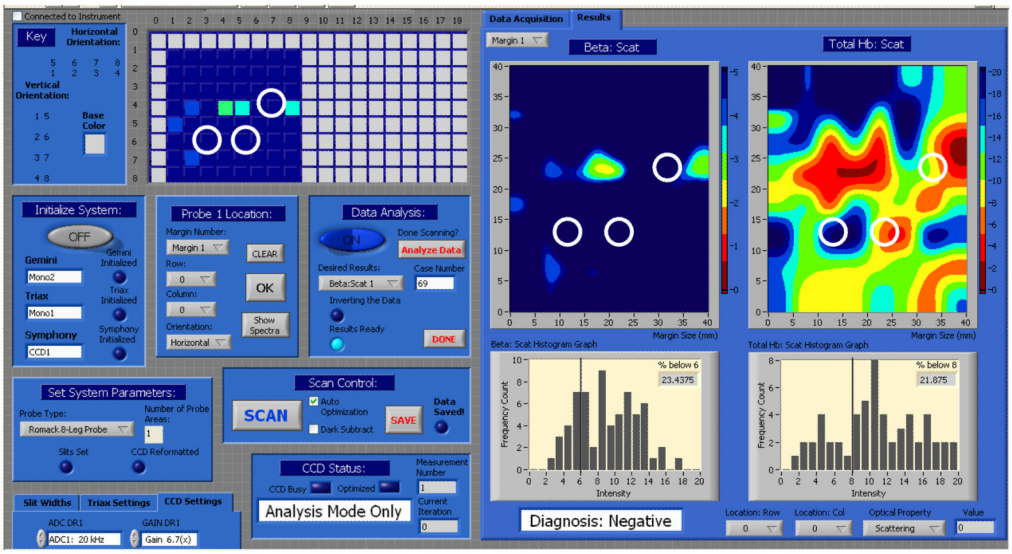

Fig. 5.

Representative results from the clinical study, showing results from a pathologically-confirmed negative margin. These screenshots depict the β-carotene:< μs′> (left) and total hemoglobin:< μs′> (right) maps, as well as the corresponding histograms for these images. The percentage of image pixels below the pre-defined thresholds are indicated in this histogram insets, and the corresponding predicted margin diagnosis is indicated at the bottom of the screen. Path-confirmed cancer-free pixels are indicated with white circles.

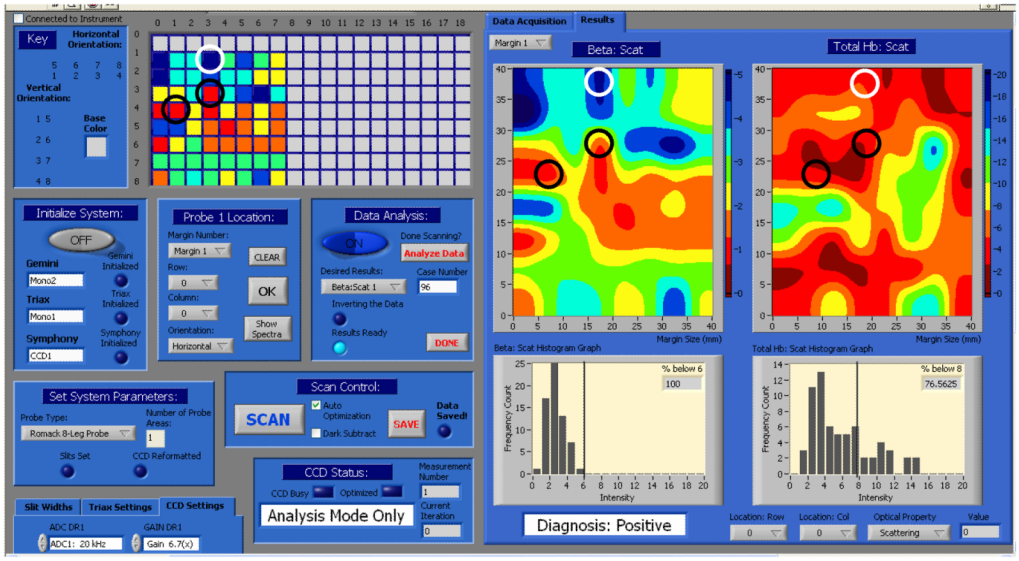

Fig. 6.

Representative results from the clinical study, showing results from a pathologically-confirmed positive margin (IDC). The black circles indicate pixels which were confirmed to contain residual invasive ductal carcinoma, whereas white circles indicate pixels which were confirmed to be free of residual cancer.

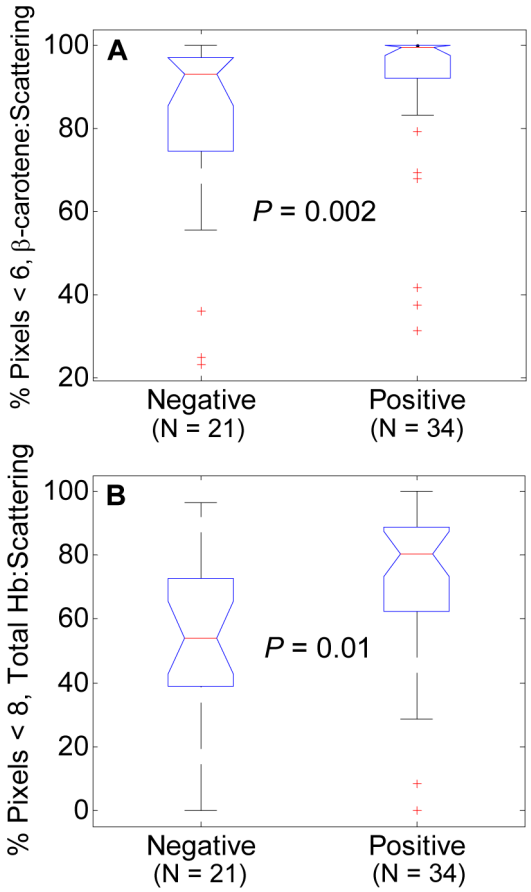

Fig. 7.

Boxplots of image-descriptive variables with highest diagnostic potential. A) Boxplot of percentage of β-carotene:< μ_s'> image pixels below 6 μM-cm, B) boxplot of percentage of total hemoglobin:< μ_s'> image pixels below 8 μM-cm. *P*-values from Wilcoxon rank-sum tests are given in the panels.

Table 1

Summary of clinical studies reporting application of optical techniques to breast tumor margin assessment.

Reference	N	Optical Technique	Implementation	Sampling Method	Max Sensing Depth	Histopathology
Bigio et al. [26]	24	ESS	*in vivo*	Discrete sites	300 μm	site-level
Haka et al. [28]	9	RS	*in vivo*	Discrete sites	n/s	site-level
Marzullo et al. [31]	18	FT-RS	*ex vivo*	Discrete sites	n/s	site-level
Keller et al. [32]	n/a	SORS	*ex vivo*	Discrete sites	2 mm	n/a
Zysk et al. [37]	2	OCT	*ex vivo*	Discrete sites	1.5 mm	site-level
This paper	48	Q-DRI	*ex vivo*	Entire margin	~2 mm	margin-level

N = number of patients, n/a = not applicable, n/s = not specified.

Table 2

Comparison of the Q-DRI device with current intra-operative techniques.

	Method/Technology		
	Touch-prep cytology	**Frozen section**	**Q-DRI**
Pathologist required in OR?	Yes	Yes	No
Percentage of margin examined	100% of surface	<1%	100% of margin
Sensing depth	Surface only	No limit	1–2mm
Problematic with fatty tissues?	No	Yes	No
Destroys tissue?	No	Yes	No
Interferes with pathology?	No	Yes	No
Time required	15–25 min	15–25 min	<20 min

Table 3

Performance of decision tree predictive model on all margins, as well as on positive or close margins only, stratified by depth of disease from the margin surface. A category of ‘Unknown’ is given to close margins in which disease depth was not explicitly specified by routine pathology.

	All Margins		Positive Margins, by Distance of Disease from Surface			
	Negative	Positive	At surface	Close, < 1mm	Close, 1–2mm	Unknown
Probe Positive	7	27	14	5	5	3
Probe Negative	14	7	3	2	1	1
Sensitivity	79.4%		82.4%	71.4%	83.3%	75.0%
Specificity	66.7%					

Table 4

Performance of decision tree predictive model on positive or close margins, stratified by disease variant found at the margin

	Positive/close margins, by diagnosis at the margin		
	IDC	**DCIS**	**Other**
Probe Positive	11	8	8
Probe Negative	3	1	3
Sensitivity	78.6%	88.9%	72.7%